A robust solver for the finite element approximation of stationary incompressible MHD equations in 3D

Lingxiao Li[a,b], Weiying Zheng[a,b,1,*]

[a]NCMIS, LSEC, Institute of Computational Mathematics and Scientific/Enginnering Computing, Academy of Mathematics and Systems Science, Chinese Academy of Sciences, Beijing, 100190, China.
[b]School of Mathematical Science, University of Chinese Academy of Sciences, Beijing, 100049, China.

Abstract

In this paper, we propose a Newton-Krylov solver and a Picard-Krylov solver for finite element discrete problem of stationary incompressible magnetohydrodynamic equations in three dimensions. Using a mixed finite element method, we discretize the velocity and the pressure by $\boldsymbol{H}^1(\Omega)$-conforming finite elements and discretize the magnetic field by $\boldsymbol{H}(\mathbf{curl}, \Omega)$-conforming edge elements. An efficient preconditioner is proposed to accelerate the convergence of GMRES method for solving linearized discrete problems. By extensive numerical experiments, we demonstrate the robustness of the Newton-Krylov solver for relatively large physical parameters and the optimality with respect to the number of degrees of freedom. Moreover, the numerical experiments show that the Newton-Krylov solver is more robust than the Picard-Krylov solver for large Reynolds number.

Keywords: Incompressible magnetohydrodynamic equations, mixed finite element method, block preconditioner, grad-div stabilization, Newton's method.

MSC: 75W05, 65F08, 65M22

1. Introduction

Magnetohydrodynamics has broad applications in our real world. It describes the interaction between electrically conducting fluid and magnetic field. It is used in industry to heat, pump, stir, and levitate liquid metals. Incompressible magnetohydrodynamic (MHD) model also governs the terrestrial magnetic filed maintained by fluid motion in the earth core and the solar magnetic field which generates sunspots and solar flares[8]. The incompressible MHD model consists of the incompressible Navier-Stokes equations and the quasi-static Maxwell equations. The magnetic field influences the momentum of the fluid through Lorentz force, and conversely, the motion of fluid influences the magnetic field through Faraday's law. In this paper,

*Corresponding author: Tel: +86-10-82541735.
Email addresses: lilingxiao@lsec.cc.ac.cn (Lingxiao Li), zwy@lsec.cc.ac.cn (Weiying Zheng)

[1]This author is supported by China NSF under the grants 91430215 and by the National Magnetic Confinement Fusion Science Program 2015GB110003..

we are studying efficient iterative solver for the stationary MHD equations

$$\boldsymbol{u}\cdot\nabla\boldsymbol{u}+\nabla p-R_e^{-1}\Delta\boldsymbol{u}-S\,\mathbf{curl}\,\boldsymbol{B}\times\boldsymbol{B}=\boldsymbol{f}\qquad\text{in }\Omega,\tag{1a}$$

$$\mathbf{curl}\left(\boldsymbol{B}\times\boldsymbol{u}+R_m^{-1}\,\mathbf{curl}\,\boldsymbol{B}\right)=0\qquad\text{in }\Omega,\tag{1b}$$

$$\operatorname{div}\boldsymbol{u}=0,\quad\operatorname{div}\boldsymbol{B}=0\qquad\text{in }\Omega,\tag{1c}$$

where $\boldsymbol{u}$ is the velocity of fluid, p is the hydrodynamic pressure, $\boldsymbol{B}$ is the magnetic induction or the magnetic field provided with constant permeability, R_e is the fluid Reynolds number, R_m is the magnetic Reynolds number, S is the coupling constant concerning Lorentz force, and $\boldsymbol{f}\in\boldsymbol{L}^2(\Omega)$ stands for external force. We assume that Ω is a bounded Lipschitz domain. The system of equations is complemented with Dirichlet boundary conditions

$$\boldsymbol{u}=\boldsymbol{g},\quad\boldsymbol{B}\times\boldsymbol{n}=\boldsymbol{B}_s\times\boldsymbol{n}\qquad\text{on }\Gamma:=\partial\Omega.\tag{2}$$

For convenience in numerical computations, we assume $\boldsymbol{g}\in\boldsymbol{H}^{1/2}(\Gamma)$ and $\boldsymbol{B}_s\in\boldsymbol{L}^2(\Gamma)$.

There are many papers in the literature on numerical solutions of incompressible MHD equations (cf. e.g. [18, 19, 21, 17, 24, 27, 29, 30, 31] and the references therein). In [21], Gunzburger et al studied the well-posedness and the finite element method for stationary MHD equations and discretized the magnetic field by $\boldsymbol{H}^1(\Omega)$-conforming finite elements. Strauss et al studied adaptive finite element method for two-dimensional (2D) MHD equations [24]. We also refer to [18] for a systematic analysis of finite element methods for incompressible MHD equations. In [39], Salah et al studied finite element approximations for both magnetic field formulation and vector potential formulation of 3D MHD equations. For the magnetic field formulation, the authors proposed two finite element methods, a stabilized finite element method and a Galerkin-least-squares finite element method. For the vector potential formulation, they proposed a Galerkin approximation using continuous finite element functions. When the domain has re-entrant angle, the magnetic field may not be in $\boldsymbol{H}^1(\Omega)$. It is preferable to use noncontinuous finite element functions to approximate $\boldsymbol{B}$, namely, the so-called edge element method [15, 28]. In 2004, Schötzau proposed a mixed finite element method to solve stationary MHD equations and discretized the magnetic field with edge elements [38].

The study on robust and efficient solvers for discretized Navier-Stokes equations or discretized MHD equations is another active research topic in computational fluid dynamics. Over the past three decades, fast solvers for incompressible Navier-Stokes equations are extensively studied in the literature (cf. e.g. [9, 10, 11, 32, 42, 43]). For moderate Reynolds number, Picard iterations for stationary impressible Navier-Stokes equation are stable and efficient. At each iteration, one needs to solve the linearized problem, or the Oseen equations,

$$\boldsymbol{w}\cdot\nabla\boldsymbol{u}+\nabla p-R_e^{-1}\Delta\boldsymbol{u}=\boldsymbol{f}\qquad\text{in }\Omega,\tag{3a}$$

$$\operatorname{div}\boldsymbol{u}=0\qquad\text{in }\Omega,\tag{3b}$$

$$\boldsymbol{u}=\boldsymbol{g}\qquad\text{on }\Gamma,\tag{3c}$$

where $\boldsymbol{w}$ stands for the approximate solution from the previous iteration. Iterative methods for solving discretized Navier-Stokes equations or discretized Oseen equations mainly consist of Krylov subspace methods [10, 22], multigrid methods [41], or their combinations [23, 34, 40]. In terms of parallel computing and practical implementation, it is preferable to use Krylov subspace method combined with an effective and robust preconditioner. Among them, the pressure convection-diffusion preconditioner [22], the least-squares commutator (LSC) preconditioner [9, 10, 11], and the augmented Lagrangian (AL) preconditioner [3, 4] prove robust and efficient for relatively large Reynolds number.

Based on an exact penalty formulation of the 2D MHD model and the $\boldsymbol{H}^1(\Omega)$-conforming finite element discretization of $\boldsymbol{B}$, Philips et al proposed a block preconditioner for solving discretized MHD equations

[35]. We also refer to the work of Adler et al [1] for monolithic multigrid Method for 2D resistive MHD equations. To our knowledge, efficient solvers for three-dimensional (3D) MHD equations are still rare in the literature, particularly, for large Reynolds number R_e and large coupling number S. An efficient solver should possess two merits:

1. the convergence rate is independent of the mesh or the number of degrees of freedom (DOFs);
2. the algorithm is robust with respect to physical parameters.

Very recently, Philips et al studied block preconditioners for 3D incompressible MHD equations [37]. They proposed a mixed finite element approximation which uses stable $\boldsymbol{Q}_2$–Q_1 finite element pair for hydrodynamics and stable edge-node finite element pair for magnetic induction problem. Block preconditioners are designed for the discrete MHD problem by using an adaptation of the LSC precontioner for discretized Navier-Stokes equations and by devising block preconditioners for mass augmented and grad-div augmented magnetic induction problems. They show numerically that the preconditioner with grad-div augmentation is more efficient and scalable for both time-dependent and stationary problems.

The objective of this paper is to propose a preconditioned GMRES method for solving linearized discrete problem of (1)–(2). We shall adopt a weak formulation of (1)–(2) which uses the grad-div or AL stabilization for the momentum equation. It is known that, for Navier-Stokes or Oseen equations, the grad-div stabilization enhances the stability of numerical solutions and yields uniform finite element error estimates with constants independent of Reynolds number [7, 12, 13, 33]. However, papers on the grad-div stabilization for MHD equations are rather rare in the literature. We discretize the Navier-Stokes equations by the Taylor-Hood $\boldsymbol{P}_2$–P_1 elements and discretize the magnetic induction equation with Nédélec's edge elements. By utilizing block structure of the full coupled system and devising approximate Schur complements, we develop a new block preconditioner for Newton's linearization of the discrete nonlinear system. The preconditioner proves to be robust when Reynolds number and coupling number are relatively large and to be optimal with respect to the number of DOFs. Different from [37] which uses the LSC preconditioner for hydrodynamics and the grad-div stabilization for magnetic induction equation, this paper uses the grad-div stabilization for hydrodynamics and approximates the resulting Schur complement by pressure mass matrix.

The paper is organized as follows: In Section 2, we introduce some notations for Sobolev spaces. A mixed finite element method is proposed to solve the AL formulation of the stationary MHD equations. In Section 3, we introduce Newton's linearization for the nonlinear discrete MHD problem and devise a robust preconditioner for solving linearized discrete problem. In Section 4, we present extensive numerical experiments to verify the optimal convergence rate of the mixed finite element method and to demonstrate the optimality and the robustness of the MHD solver. In Section 5, we made some conclusions on the preconditioner presented in this paper. Throughout the paper we shall denote vector-valued quantities by boldface notation, such as $\boldsymbol{L}^2(\Omega) := (L^2(\Omega))^3$.

2. Mixed finite element method for the MHD equations

First we introduce some Sobolev spaces and norms used in this paper. Let $L^2(\Omega)$ be the usual Hilbert space of square integrable functions which is equipped with the following inner product and norm:

$$(u, v) := \int_\Omega u(\boldsymbol{x})\, v(\boldsymbol{x}) \mathrm{d}\boldsymbol{x} \quad \text{and} \quad \|u\|_{L^2(\Omega)} := (u, u)^{1/2}.$$

Let the quotient space of $L^2(\Omega)$ be defined by

$$L_0^2(\Omega) := \left\{ v \in L^2(\Omega) \ : \ (v, 1) = 0 \right\} = L^2(\Omega)/\mathbb{R} \, .$$

Define $H^m(\Omega) := \{v \in L^2(\Omega) : D^\xi v \in L^2(\Omega), |\xi| \le m\}$ where ξ represents non-negative triple index. Let $H_0^1(\Omega)$ be the subspace of $H^1(\Omega)$ whose functions have zero traces on Γ.

We define the spaces of functions having square integrable curl by

$$\begin{aligned} \boldsymbol{H}(\mathbf{curl}, \Omega) &:= \{\boldsymbol{v} \in \boldsymbol{L}^2(\Omega) : \mathbf{curl}\, \boldsymbol{v} \in \boldsymbol{L}^2(\Omega)\}, \\ \boldsymbol{H}_0(\mathbf{curl}, \Omega) &:= \{\boldsymbol{v} \in \boldsymbol{H}(\mathbf{curl}, \Omega) : \boldsymbol{n} \times \boldsymbol{v} = 0 \ \text{ on } \Gamma\}, \end{aligned}$$

which are equipped with the following inner product and norm

$$(\boldsymbol{v}, \boldsymbol{w})_{\boldsymbol{H}(\mathbf{curl},\Omega)} := (\boldsymbol{v}, \boldsymbol{w}) + (\mathbf{curl}\, \boldsymbol{v}, \mathbf{curl}\, \boldsymbol{w}), \qquad \|\boldsymbol{v}\|_{\boldsymbol{H}(\mathbf{curl},\Omega)} := \sqrt{(\boldsymbol{v}, \boldsymbol{v})_{\boldsymbol{H}(\mathbf{curl},\Omega)}}\,.$$

Here $\boldsymbol{n}$ denotes the unit outer normal to Ω.

Inspired by [33, 38], we introduce a Lagrange multiplier r and rewrite (1) into an AL form

$$\boldsymbol{u} \cdot \nabla \boldsymbol{u} + \nabla p - \gamma \nabla \operatorname{div} \boldsymbol{u} - R_e^{-1} \Delta \boldsymbol{u} - S\, \mathbf{curl}\, \boldsymbol{B} \times \boldsymbol{B} = \boldsymbol{f} \qquad \text{in } \Omega, \tag{4a}$$

$$S\, \mathbf{curl} \left(\boldsymbol{B} \times \boldsymbol{u} + R_m^{-1}\, \mathbf{curl}\, \boldsymbol{B} \right) + \nabla r = 0 \qquad \text{in } \Omega, \tag{4b}$$

$$\operatorname{div} \boldsymbol{u} = 0, \qquad \operatorname{div} \boldsymbol{B} = 0 \qquad \text{in } \Omega, \tag{4c}$$

$$\boldsymbol{u} = \boldsymbol{g}, \quad \boldsymbol{B} \times \boldsymbol{n} = \boldsymbol{B}_s \times \boldsymbol{n}, \quad r = 0 \qquad \text{on } \Gamma. \tag{4d}$$

where $\gamma > 0$ is the stabilization parameter or penalty parameter. Taking divergence on both sides of (4b) and using (4d) yields

$$\Delta r = 0 \quad \text{in } \Omega, \qquad r = 0 \quad \text{in } \Gamma.$$

This means $r = 0$ in Ω actually. Since $\operatorname{div} \boldsymbol{u} = 0$, (4) is equivalent to (1)–(2). In the rest of this paper, we are going to study the AL problem (4) instead of the original problem.

A weak formulation of (4) reads: Find $(\boldsymbol{u}, \boldsymbol{B}) \in \boldsymbol{H}^1(\Omega) \times \boldsymbol{H}(\mathbf{curl}, \Omega)$ and $(p, r) \in L_0^2(\Omega) \times H_0^1(\Omega)$ such that $\boldsymbol{u} = \boldsymbol{g}$ and $\boldsymbol{B} \times \boldsymbol{n} = \boldsymbol{B}_s \times \boldsymbol{n}$ on Γ and

$$\mathcal{A}((\boldsymbol{u}, \boldsymbol{B}), (\boldsymbol{v}, \boldsymbol{\varphi})) + \mathcal{O}((\boldsymbol{u}, \boldsymbol{B}); (\boldsymbol{u}, \boldsymbol{B}), (\boldsymbol{v}, \boldsymbol{\varphi})) - \mathcal{B}((p, r), (\boldsymbol{v}, \boldsymbol{\varphi})) = (\boldsymbol{f}, \boldsymbol{v}), \tag{5a}$$

$$-\mathcal{B}((q, s), (\boldsymbol{u}, \boldsymbol{B})) = 0, \tag{5b}$$

for all $(\boldsymbol{v}, \boldsymbol{\varphi}) \in \boldsymbol{H}_0^1(\Omega) \times \boldsymbol{H}_0(\mathbf{curl}, \Omega)$ and $(q, s) \in L_0^2(\Omega) \times H_0^1(\Omega)$, where the bilinear forms and trilinear form are defined respectively by

$$\begin{aligned} \mathcal{A}((\boldsymbol{u}, \boldsymbol{B}), (\boldsymbol{v}, \boldsymbol{\varphi})) &= R_e^{-1}(\nabla \boldsymbol{u}, \nabla \boldsymbol{v}) + \gamma(\operatorname{div} \boldsymbol{u}, \operatorname{div} \boldsymbol{v}) + S R_m^{-1}(\nabla \times \boldsymbol{B}, \nabla \times \boldsymbol{\varphi}), \\ \mathcal{O}((\boldsymbol{w}, \boldsymbol{\psi}); (\boldsymbol{u}, \boldsymbol{B}), (\boldsymbol{v}, \boldsymbol{\varphi})) &= (\boldsymbol{w} \cdot \nabla \boldsymbol{u}, \boldsymbol{v}) - S \left[(\mathbf{curl}\, \boldsymbol{B}, \boldsymbol{\psi} \times \boldsymbol{v}) - (\boldsymbol{\psi} \times \boldsymbol{u}, \mathbf{curl}\, \boldsymbol{\varphi}) \right], \\ \mathcal{B}((p, r), (\boldsymbol{v}, \boldsymbol{\varphi})) &= (p, \operatorname{div} \boldsymbol{v}) + (\nabla r, \boldsymbol{\varphi}). \end{aligned}$$

Assuming small data, Schötzau proved the existence and uniqueness of the solution to (5) without the grad-div stabilization term $\gamma(\operatorname{div} \boldsymbol{u}, \operatorname{div} \boldsymbol{v})$ [38]. For the Navier-Stokes or Oseen equations, the grad-div stabilization enhances the stability of numerical solutions and yields uniform finite element error estimates with constants independent of Reynolds number [7, 12, 13, 33], but has not been well-studied for MHD equations. The purpose of this paper is to propose a robust solver for the discrete problem of (5). We do not elaborate on the well-posedness of this model.

Now we introduce the finite element approximation to (5). Let $\mathcal{T}_h$ be a quasi-uniform and shape-regular tetrahedral mesh of Ω. Let h denote the maximal diameter of all tetrahedra on the mesh. For any $T \in \mathcal{T}_h$, let

$P_k(T)$ be the space of polynomials of degree $k \geq 0$ on T and $\boldsymbol{P}_k(T) = (P_k(T))^3$ be the corresponding space of vector polynomials. Define the Lagrange finite element space of the k-th order by

$$V(k, \mathcal{T}_h) = \left\{ v \in H^1(\Omega) : \ v|_T \in P_k(T), \ \forall\, T \in \mathcal{T}_h \right\}.$$

First we choose the well-known Taylor-Hood $\boldsymbol{P}_2$-P_1 elements [5, Page 217-219] for the discretization of $(\boldsymbol{u}, p)$, namely,

$$\boldsymbol{V}_h := V(2, \mathcal{T}_h)^3 \cap \boldsymbol{H}_0^1(\Omega), \qquad Q_h := V(1, \mathcal{T}_h)\,.$$

From [5, Page 255-258], the discrete inf-sup condition holds

$$\sup_{0 \neq \boldsymbol{v} \in \boldsymbol{V}_h} \frac{(q, \operatorname{div} \boldsymbol{v})}{\|\boldsymbol{v}\|_{H^1(\Omega)}} \geq C_u \, \|q\|_{L^2(\Omega)} \qquad \forall\, q \in Q_h, \tag{6}$$

where $C_u > 0$ is the inf-sup constant depending only on Ω. We shall also use $\overline{\boldsymbol{V}}_h = V(2, \mathcal{T}_h)^3$.

The finite element space for $\boldsymbol{B}$ is chosen as the first order Nédélec edge element space in the second family [28], namely,

$$\overline{\boldsymbol{C}}_h = \{\boldsymbol{v} \in \boldsymbol{H}(\mathbf{curl}, \Omega) : \ \boldsymbol{v}|_T \in \boldsymbol{P}_1(T), \ \forall\, T \in \mathcal{T}_h\}, \qquad \boldsymbol{C}_h = \overline{\boldsymbol{C}}_h \cap \boldsymbol{H}_0(\mathbf{curl}, \Omega).$$

The finite element space for r is defined by

$$S_h = V(2, \mathcal{T}_h) \cap H_0^1(\Omega).$$

Since $\nabla S_h \subset \boldsymbol{C}_h$, we easily get the inf-sup condition for the pair of finite element spaces $\boldsymbol{C}_h \times S_h$

$$\sup_{0 \neq \boldsymbol{v} \in \boldsymbol{C}_h} \frac{(\nabla s, \boldsymbol{v})}{\|\boldsymbol{v}\|_{\boldsymbol{H}(\mathbf{curl}, \Omega)}} \geq |s|_{H^1(\Omega)} \geq C_b \|s\|_{H^1(\Omega)} \qquad \forall\, s \in S_h, \tag{7}$$

where $C_b > 0$ is the Poincáre constant depending only on Ω.

The finite element approximation to (5) reads: Find $(\boldsymbol{u}_h, \boldsymbol{B}_h) \in \overline{\boldsymbol{V}}_h \times \overline{\boldsymbol{C}}_h$ and $(p_h, r_h) \in Q_h \times S_h$ such that

$$\mathcal{A}((\boldsymbol{u}_h, \boldsymbol{B}_h), (\boldsymbol{v}, \boldsymbol{\varphi})) + \mathcal{O}((\boldsymbol{u}_h, \boldsymbol{B}_h); (\boldsymbol{u}_h, \boldsymbol{B}_h), (\boldsymbol{v}, \boldsymbol{\varphi})) - \mathcal{B}((p_h, r_h), (\boldsymbol{v}, \boldsymbol{\varphi})) = (\boldsymbol{f}, \boldsymbol{v}), \tag{8a}$$

$$-\mathcal{B}((q, s), (\boldsymbol{u}_h, \boldsymbol{B}_h)) = 0, \tag{8b}$$

for all $(\boldsymbol{v}, \boldsymbol{\varphi}) \in \boldsymbol{V}_h \times \boldsymbol{C}_h$ and $(q, s) \in Q_h \times S_h$. From (6) and (7) we know that the bilinear form $\mathcal{B}(\cdot, \cdot)$ satisfies the discrete inf-sup condition

$$\sup_{(\boldsymbol{v}_h, \boldsymbol{\varphi}_h) \in \boldsymbol{V}_h \times \boldsymbol{C}_h} \frac{\mathcal{B}((q_h, s_h), (\boldsymbol{v}_h, \boldsymbol{\varphi}_h))}{\|(\boldsymbol{v}_h, \boldsymbol{\varphi}_h)\|_{\boldsymbol{V}_h \times \boldsymbol{C}_h}} \geq \min(C_u, C_b) \, \|(q_h, s_h)\|_{Q_h \times S_h} \quad \forall\, (q_h, s_h) \in Q_h \times S_h\,, \tag{9}$$

where

$$\|(\boldsymbol{v}_h, \boldsymbol{\varphi}_h)\|_{\boldsymbol{V}_h \times \boldsymbol{C}_h} := \sqrt{\|\boldsymbol{v}_h\|^2_{\boldsymbol{H}^1(\Omega)} + \|\boldsymbol{\varphi}_h\|^2_{\boldsymbol{H}(\mathbf{curl}, \Omega)}}\,, \qquad \|(q_h, s_h)\|_{Q_h \times S_h} := \sqrt{\|q_h\|^2_{L^2(\Omega)} + \|s_h\|^2_{H^1(\Omega)}}\,.$$

Since we are interested in developing fast solvers for the discrete problem, we do note elaborate on the well-posedness of (8) and simply assume that it has a unique solution.

We end this section by fixing the value of γ for the grad-div stabilization term. By Example 3 in Section 4, we show numerically that our MHD solver to be proposed later is insensitive to $\gamma = O(1)$. For convenience, *we recommend to use* $\gamma = 1$.

3. A preconditioner for linearized finite element problem

In this section, we are going to study the solution of the nonlinear discrete problem (8). First we propose both Newton's linearization and Picard's linearization for (8). The preconditioner for the linearized MHD equations depends crucially on both the preconditioner for the AL Navier-Stokes equations and the preconditioner for Maxwell's equations.

3.1. Newton's and Picard's methods for the discrete MHD equations

In this subsection, we consider linearizations of (8). Let $(\boldsymbol{B}_k, r_k, \boldsymbol{u}_k, p_k) \in \overline{\boldsymbol{C}}_h \times S_h \times \overline{\boldsymbol{V}}_h \times Q_h$ be the approximate solutions of (8) at the k-th iteration. The residual equations for the approximate solutions read: Find $(\delta\boldsymbol{B}, \delta r, \delta\boldsymbol{u}, \delta p) \in \boldsymbol{C}_h \times S_h \times \boldsymbol{V}_h \times Q_h$ such that

$$S R_m^{-1}(\mathbf{curl}\,\delta\boldsymbol{B}, \mathbf{curl}\,\boldsymbol{\varphi}) + (\nabla\delta r, \boldsymbol{\varphi}) + S(\boldsymbol{B}_k \times \delta\boldsymbol{u}, \mathbf{curl}\,\boldsymbol{\varphi}) + \eta S(\delta\boldsymbol{B} \times \boldsymbol{u}_k, \mathbf{curl}\,\boldsymbol{\varphi}) = R_B(\boldsymbol{\varphi}), \tag{10a}$$

$$(\delta\boldsymbol{B}, \nabla s) = R_r(s), \tag{10b}$$

$$-S(\mathbf{curl}\,\delta\boldsymbol{B}, \boldsymbol{B}_k \times \boldsymbol{v}) - \eta S(\mathbf{curl}\,\boldsymbol{B}_k, \delta\boldsymbol{B} \times \boldsymbol{v}) + \mathcal{F}(\boldsymbol{u}_k; \delta\boldsymbol{u}, \boldsymbol{v}) - (\delta p, \operatorname{div}\boldsymbol{v}) = R_u(\boldsymbol{v}), \tag{10c}$$

$$-(\operatorname{div}\delta\boldsymbol{u}, q) = R_p(q), \tag{10d}$$

where the trilinear form $\mathcal{F}$ represents the convection-diffusion part of the fluid equation

$$\mathcal{F}(\boldsymbol{u}_k; \delta\boldsymbol{u}, \boldsymbol{v}) := R_e^{-1}(\nabla\delta\boldsymbol{u}, \nabla\boldsymbol{v}) + (\boldsymbol{u}_k \cdot \nabla\delta\boldsymbol{u}, \boldsymbol{v}) + \eta(\delta\boldsymbol{u} \cdot \nabla\boldsymbol{u}_k, \boldsymbol{v}) + \gamma(\operatorname{div}\delta\boldsymbol{u}, \operatorname{div}\boldsymbol{v}),$$

and the residual functionals are defined by

$$\begin{aligned}
&R_B(\boldsymbol{\varphi}) = -S R_m^{-1}(\mathbf{curl}\,\boldsymbol{B}_k, \mathbf{curl}\,\boldsymbol{\varphi}) - (\nabla r_k, \boldsymbol{\varphi}) - S(\boldsymbol{B}_k \times \boldsymbol{u}_k, \mathbf{curl}\,\boldsymbol{\varphi}),\\
&R_r(s) = -(\boldsymbol{B}_k, \nabla s),\\
&R_u(\boldsymbol{v}) = (\boldsymbol{f}, \boldsymbol{v}) - R_e^{-1}(\nabla\boldsymbol{u}_k, \nabla\boldsymbol{v}) - (\boldsymbol{u}_k \cdot \nabla\boldsymbol{u}_k, \boldsymbol{v}) - \gamma(\operatorname{div}\boldsymbol{u}_k, \operatorname{div}\boldsymbol{v}) + S(\mathbf{curl}\,\boldsymbol{B}_k, \boldsymbol{B}_k \times \boldsymbol{v}) + (p_k, \operatorname{div}\boldsymbol{v}),\\
&R_p(q) = (\operatorname{div}\boldsymbol{u}_k, q).
\end{aligned}$$

The linearization represents Newton's method when $\eta = 1$ and Picard's method when $\eta = 0$. After solving (10), the approximate solutions will be updated by

$$\boldsymbol{B}_{k+1} = \boldsymbol{B}_k + \theta\,\delta\boldsymbol{B}, \quad r_{k+1} = r_k + \theta\,\delta r, \quad \boldsymbol{u}_{k+1} = \boldsymbol{u}_k + \theta\,\delta\boldsymbol{u}, \quad p_{k+1} = p_k + \theta\,\delta p \tag{11}$$

with a relaxation factor $0 < \theta \leq 1$.

To devise the preconditioner, we write problem (10) into an algebraic form

$$\mathbb{A}\mathbf{x} = \mathbf{b}. \tag{12}$$

In block forms, they can be written as

$$\mathbf{x} = \begin{pmatrix} \mathbf{x}_B \\ \mathbf{x}_r \\ \mathbf{x}_u \\ \mathbf{x}_p \end{pmatrix}, \qquad \mathbf{b} = \begin{pmatrix} \mathbf{b}_B \\ \mathbf{b}_r \\ \mathbf{b}_u \\ \mathbf{b}_p \end{pmatrix}, \qquad \mathbb{A} = \begin{pmatrix} \mathbb{C} & \mathbb{G}^\top & \mathbb{J}^\top & 0 \\ \mathbb{G} & 0 & 0 & 0 \\ -\mathbb{K} & 0 & \mathbb{F} & \mathbb{B}^\top \\ 0 & 0 & \mathbb{B} & 0 \end{pmatrix}, \tag{13}$$

where $\mathbf{x}_B, \mathbf{x}_r, \mathbf{x}_u, \mathbf{x}_p$ are vectors representing degrees of freedom for $\delta\boldsymbol{B}, \delta r, \delta\boldsymbol{u}, \delta p$ respectively and $\mathbf{b}_B, \mathbf{b}_r, \mathbf{b}_u, \mathbf{b}_p$ are the corresponding residual vectors. Let $\{\boldsymbol{v}_i : 1 \leq i \leq N_V\}$, $\{\boldsymbol{\varphi}_i : 1 \leq i \leq N_C\}$, $\{q_i : 1 \leq i \leq N_Q\}$,

$\{s_i : 1 \le i \le N_S\}$ be the bases of $\boldsymbol{V}_h$, $\boldsymbol{C}_h$, Q_h, and S_h respectively. Then the entries of all block matrices of $\mathbb{A}$ are defined by

$$
\begin{aligned}
\mathbb{C}_{ij} &= S R_m^{-1}(\mathbf{curl}\,\boldsymbol{\varphi}_j, \mathbf{curl}\,\boldsymbol{\varphi}_i) + \eta S(\boldsymbol{\varphi}_j \times \boldsymbol{u}_k, \mathbf{curl}\,\boldsymbol{\varphi}_i),\\
\mathbb{G}_{ij} &= (\boldsymbol{\varphi}_j, \nabla s_i),\\
\mathbb{J}_{ij} &= S(\mathbf{curl}\,\boldsymbol{\varphi}_j, \boldsymbol{B}_k \times \boldsymbol{v}_i),\\
\mathbb{K}_{ij} &= \mathbb{J}_{ij} + \eta S(\mathbf{curl}\,\boldsymbol{B}_k, \boldsymbol{\varphi}_j \times \boldsymbol{v}_i),\\
\mathbb{F}_{ij} &= \mathcal{F}(\boldsymbol{u}_k; \boldsymbol{v}_j, \boldsymbol{v}_i),\\
\mathbb{B}_{ij} &= -(\operatorname{div} \boldsymbol{v}_j, q_i).
\end{aligned}
$$

Clearly the block matrices represent the differential operators appearing in the Navier-Stokes equations and Maxwell's equations on various finite element spaces

$$
\begin{aligned}
\mathbb{C} \Leftrightarrow S R_m^{-1}\,\mathbf{curl}\,\mathbf{curl} + \eta S\,\mathbf{curl}(*\times \boldsymbol{u}_k), \quad \mathbb{G} &\Leftrightarrow -\operatorname{div} \quad \text{on } \boldsymbol{C}_h,\\
\mathbb{G}^\top &\Leftrightarrow \nabla \quad \text{on } S_h,\\
\mathbb{F} \Leftrightarrow -R_e^{-1}\Delta + \boldsymbol{u}_k\cdot\nabla + \eta(*\cdot\nabla)\boldsymbol{u}_k - \gamma\nabla\operatorname{div}, \quad \mathbb{B} &\Leftrightarrow -\operatorname{div} \quad \text{on } \boldsymbol{V}_h,\\
\mathbb{B}^\top &\Leftrightarrow \nabla \quad \text{on } Q_h.
\end{aligned}
$$

Here $(-\operatorname{div})$ is understood as the dual operator of $\nabla|_{S_h}$ or $\nabla|_{Q_h}$. Moreover, $\mathbb{K}, \mathbb{J}^\top$ are algebraic representations of the two multiplication operators which couple the magnetic field and the conducting fluid. For any given $\boldsymbol{v}_h \in \boldsymbol{V}_h$ and $\boldsymbol{\varphi}_h \in \boldsymbol{C}_h$, we have

$$
\mathbb{J}^\top \Leftrightarrow S\,\mathbf{curl}(\boldsymbol{B}_k \times \boldsymbol{v}_h) \quad \text{on } \boldsymbol{C}_h, \qquad \mathbb{K} \Leftrightarrow S\,\mathbf{curl}\,\boldsymbol{\varphi}_h \times \boldsymbol{B}_k + \eta S\,\mathbf{curl}\,\boldsymbol{B}_k \times \boldsymbol{\varphi}_h \quad \text{on } \boldsymbol{V}_h. \tag{14}
$$

The relationships between these operators play an important role in devising a robust preconditioner for the linearized problem.

3.2. Preconditioning for the linearized MHD equations

Now we study the preconditioner for matrix $\mathbb{A}$. The main idea is to use matrix decompositions and spectral equivalences in simplifying matrices. Let $\mathbb{L}_r$ be the stiffness matrix of $-\Delta$ on S_h and let $\sigma > 0$ be a relaxation parameter whose value will be fixed later in Section 3.5 (see equation (33)). First we pre-multiply the second row of $\mathbb{A}$ by $\sigma\mathbb{G}^\top\mathbb{L}_r^{-1}$ and add it to the first row. This yields a decomposition of $\mathbb{A}$

$$
\mathbb{A} = \mathbb{P}_1\mathbb{A}_1 \equiv \begin{pmatrix} \mathbb{I} & -\sigma\mathbb{G}^\top\mathbb{L}_r^{-1} & 0 & 0\\ 0 & \mathbb{I} & 0 & 0\\ 0 & 0 & \mathbb{I} & 0\\ 0 & 0 & 0 & \mathbb{I} \end{pmatrix} \begin{pmatrix} \hat{\mathbb{C}} & \mathbb{G}^\top & \mathbb{J}^\top & 0\\ \mathbb{G} & 0 & 0 & 0\\ -\mathbb{K} & 0 & \mathbb{F} & \mathbb{B}^\top\\ 0 & 0 & \mathbb{B} & 0 \end{pmatrix}, \tag{15}
$$

where $\hat{\mathbb{C}} = \mathbb{C} + \sigma\mathbb{S}_r$ and $\mathbb{S}_r := \mathbb{G}^\top\mathbb{L}_r^{-1}\mathbb{G}$. We further pre-multiply the first row of $\mathbb{A}_1$ by $-\mathbb{G}\hat{\mathbb{C}}^{-1}$ and add it to the second row. This yields a decomposition of $\mathbb{A}_1$

$$
\mathbb{A}_1 = \mathbb{P}_2\mathbb{A}_2 = \begin{pmatrix} \mathbb{I} & 0 & 0 & 0\\ \mathbb{G}\hat{\mathbb{C}}^{-1} & \mathbb{I} & 0 & 0\\ 0 & 0 & \mathbb{I} & 0\\ 0 & 0 & 0 & \mathbb{I} \end{pmatrix} \begin{pmatrix} \hat{\mathbb{C}} & \mathbb{G}^\top & \mathbb{J}^\top & 0\\ 0 & -\mathbb{G}\hat{\mathbb{C}}^{-1}\mathbb{G}^\top & -\mathbb{G}\hat{\mathbb{C}}^{-1}\mathbb{J}^\top & 0\\ -\mathbb{K} & 0 & \mathbb{F} & \mathbb{B}^\top\\ 0 & 0 & \mathbb{B} & 0 \end{pmatrix}. \tag{16}
$$

Note that $\mathbb{G}\mathbb{M}^{-1}\hat{\mathbb{C}}$ represents the operator $-\operatorname{div}\left(S R_m^{-1}\,\mathbf{curl}\,\mathbf{curl}+\sigma\nabla\Delta^{-1}\operatorname{div}\right)$ where $\mathbb{M}$ is the mass matrix on $\boldsymbol{C}_h$. Since

$$\operatorname{div}\left(S R_m^{-1}\,\mathbf{curl}\,\mathbf{curl}+\sigma\nabla\Delta^{-1}\operatorname{div}\right) = \sigma\Delta\Delta^{-1}\operatorname{div} = \sigma\operatorname{div}.$$

This means that

$$\mathbb{G}\mathbb{M}^{-1}\hat{\mathbb{C}} \approx \sigma\mathbb{G} \qquad \text{and} \qquad \mathbb{G}\hat{\mathbb{C}}^{-1} \approx \sigma^{-1}\mathbb{G}\hat{\mathbb{M}}^{-1}.$$

Since $\mathbb{J}^\top$ represents the coupling term $\mathbf{curl}(S\boldsymbol{B}_k \times \boldsymbol{v}_h)$, we have $\mathbb{G}\mathbb{M}^{-1}\mathbb{J}^\top \approx 0$. Therefore,

$$\mathbb{G}\hat{\mathbb{C}}^{-1}\mathbb{J}^\top \approx 0, \qquad \mathbb{G}\hat{\mathbb{C}}^{-1}\mathbb{G}^\top \approx \sigma^{-1}\mathbb{G}\mathbb{M}^{-1}\mathbb{G}^\top \approx \sigma^{-1}\mathbb{L}_r.$$

For Picard's linearization ($\eta = 0$), from [20], we know that $\mathbb{C}+\sigma\mathbb{M}$ is equivalent to $\mathbb{C}+\sigma\mathbb{S}_r$ in spectrum. For Newton's linearization ($\eta = 1$), the equivalence can not be obtained easily. However, numerical evidences in [36] show that we can still use the approximation

$$\mathbb{C}_\sigma := \mathbb{C} + \sigma\mathbb{M} \approx \mathbb{C} + \sigma\mathbb{S}_r$$

in constructing preconditioners. Combining the above approximations with (15) and (16), we obtain

$$\mathbb{A} \approx \mathbb{P}_1\mathbb{P}_2 \begin{pmatrix} \mathbb{C}_\sigma & \mathbb{G}^\top & \mathbb{J}^\top & 0 \\ 0 & -\sigma^{-1}\mathbb{L}_r & 0 & 0 \\ -\mathbb{K} & 0 & \mathbb{F} & \mathbb{B}^\top \\ 0 & 0 & \mathbb{B} & 0 \end{pmatrix} = \mathbb{P}_1\mathbb{P}_2\mathbb{P}_3\mathbb{A}_3, \tag{17}$$

where

$$\mathbb{P}_3 = \begin{pmatrix} \mathbb{I} & 0 & 0 & 0 \\ 0 & \mathbb{I} & 0 & 0 \\ -\mathbb{K}\mathbb{C}_\sigma^{-1} & -\sigma\mathbb{K}\mathbb{C}_\sigma^{-1}\mathbb{G}^\top\mathbb{L}_r^{-1} & \mathbb{I} & 0 \\ 0 & 0 & 0 & \mathbb{I} \end{pmatrix}, \quad \mathbb{A}_3 = \begin{pmatrix} \mathbb{C}_\sigma & \mathbb{G}^\top & \mathbb{J}^\top & 0 \\ 0 & -\sigma^{-1}\mathbb{L}_r & 0 & 0 \\ 0 & 0 & \mathbb{F}+\mathbb{K}\mathbb{C}_\sigma^{-1}\mathbb{J}^\top & \mathbb{B}^\top \\ 0 & 0 & \mathbb{B} & 0 \end{pmatrix}.$$

This shows that $\mathbb{A}(\mathbb{P}_1\mathbb{A}_3)^{-1} \approx \mathbb{P}_1(\mathbb{P}_2\mathbb{P}_3)\mathbb{P}_1^{-1}$. The right-hand side is similar to $\mathbb{P}_2\mathbb{P}_3$ and then has the same minimum polynomial. Since $\mathbb{P}_2\mathbb{P}_3$ only has the unit eigenvalue, the inverse of $\mathbb{A}_4 := \mathbb{P}_1\mathbb{A}_3$ can readily serve as a right preconditioner for $\mathbb{A}$. Direct calculations show that

$$\mathbb{A}_4 = \begin{pmatrix} \mathbb{C}_\sigma & 2\mathbb{G}^\top & \mathbb{J}^\top & 0 \\ 0 & -\sigma^{-1}\mathbb{L}_r & 0 & 0 \\ 0 & 0 & \mathbb{F}+\mathbb{K}\mathbb{C}_\sigma^{-1}\mathbb{J}^\top & \mathbb{B}^\top \\ 0 & 0 & \mathbb{B} & 0 \end{pmatrix}. \tag{18}$$

We still have the difficulties in computing the inverse of $\mathbb{F}+\mathbb{K}\mathbb{C}_\sigma^{-1}\mathbb{J}^\top$. Next we are going to derive a good approximation of $\mathbb{F}+\mathbb{K}\mathbb{C}_\sigma^{-1}\mathbb{J}^\top$ so that its inverse is easy to compute.

3.3. A preconditioner for the magnetic field-fluid coupling block of Picard's linearization

From (18), the key step to compute $\mathbb{A}_4^{-1}$ is how to precondition the 2×2 block

$$\mathbb{X} = \begin{pmatrix} \mathbb{C}_\sigma & \mathbb{J}^\top \\ 0 & \mathbb{F}+\mathbb{K}\mathbb{C}_\sigma^{-1}\mathbb{J}^\top \end{pmatrix}. \tag{19}$$

We note that $\mathbb{F} + \mathbb{K}\mathbb{C}_\sigma^{-1}\mathbb{J}^\top$ is the precise Schur complement of the following matrix which accounts for the coupling between $\delta\boldsymbol{B}$ and $\delta\boldsymbol{u}$

$$\hat{\mathbb{X}} = \begin{pmatrix} \mathbb{C}_\sigma & \mathbb{J}^\top \\ -\mathbb{K} & \mathbb{F} \end{pmatrix}. \tag{20}$$

In this subsection, we are going to derive a preconditioner for the magnetic field-fluid coupling matrix $\mathbb{X}$ or $\hat{\mathbb{X}}$. We only consider Picard's linearization, namely, $\eta = 0$. This means that $\mathbb{K} = \mathbb{J}$ and $\mathbb{C}_\sigma$ is the algebraic representation of the operator $SR_m^{-1}\,\mathbf{curl}\,\mathbf{curl} + \sigma\mathbf{I}$ on $\boldsymbol{C}_h$ where $\mathbf{I}$ is the identity operator.

For $\eta = 0$, $\mathbb{J}^\top$ and $\mathbb{K}$ represent the two multiplication operators $S\,\mathbf{curl}(\boldsymbol{B}_k \times \boldsymbol{v}_h)$ and $S\,\mathbf{curl}\,\boldsymbol{\varphi}_h \times \boldsymbol{B}_k$ respectively for any given $\boldsymbol{v}_h$ and $\boldsymbol{\varphi}_h$. Let $\{\boldsymbol{v}_1, \cdots, \boldsymbol{v}_{N_V}\}$ be the basis of $\boldsymbol{V}_h$ given in Section 3.1 and write

$$\boldsymbol{v}_h = \sum_{i=1}^{N_V} \alpha_i \boldsymbol{v}_i, \qquad \mathbf{v} = (\alpha_1, \cdots, \alpha_{N_V})^\top.$$

Then $\mathbb{K}\mathbb{C}_\sigma^{-1}\mathbb{J}^\top\mathbf{v}$ is the algebraic representation of

$$S\,\mathbf{curl}\left\{\left(SR_m^{-1}\,\mathbf{curl}\,\mathbf{curl} + \sigma\mathbf{I}\right)^{-1} S\,\mathbf{curl}(\boldsymbol{B}_k \times \boldsymbol{v}_h)\right\} \times \boldsymbol{B}_k. \tag{21}$$

Since $(SR_m^{-1}\,\mathbf{curl}\,\mathbf{curl} + \sigma\mathbf{I})^{-1}$ commutates with $\mathbf{curl}$, (21) becomes

$$S^2\left\{\left(SR_m^{-1}\,\mathbf{curl}\,\mathbf{curl} + \sigma\mathbf{I}\right)^{-1}\mathbf{curl}\,\mathbf{curl}(\boldsymbol{B}_k \times \boldsymbol{v}_h)\right\} \times \boldsymbol{B}_k.$$

For $\sigma > 0$ sufficiently small, we adopt the following approximation

$$\mathbf{curl}\,\mathbf{curl} \approx S^{-1}R_m(SR_m^{-1}\,\mathbf{curl}\,\mathbf{curl} + \sigma\mathbf{I}).$$

This yields an approximation of (21)

$$S^2\left\{\left(SR_m^{-1}\,\mathbf{curl}\,\mathbf{curl} + \sigma\mathbf{I}\right)^{-1}\mathbf{curl}\,\mathbf{curl}(\boldsymbol{B}_k \times \boldsymbol{v}_h)\right\} \times \boldsymbol{B}_k \approx SR_m(\boldsymbol{B}_k \times \boldsymbol{v}_h) \times \boldsymbol{B}_k. \tag{22}$$

Therefore, we get an approximation of the Schur complement

$$\mathbb{F} + \mathbb{K}\mathbb{C}_\sigma^{-1}\mathbb{J}^\top \approx \mathbb{S},$$

where $\mathbb{S}$ is the stiffness matrix associated with the bilinear form

$$\mathcal{F}(\boldsymbol{u}_k; \delta\boldsymbol{u}, \boldsymbol{v}) + SR_m(\boldsymbol{B}_k \times \delta\boldsymbol{u}, \boldsymbol{B}_k \times \boldsymbol{v}). \tag{23}$$

This yields an approximation of $\mathbb{X}$, that is,

$$\begin{pmatrix} \mathbb{C}_\sigma & \mathbb{J}^\top \\ 0 & \mathbb{F} + \mathbb{K}\mathbb{C}_\sigma^{-1}\mathbb{J}^\top \end{pmatrix} \approx \begin{pmatrix} \mathbb{C}_\sigma & \mathbb{J}^\top \\ 0 & \mathbb{S} \end{pmatrix}. \tag{24}$$

We also refer to [35, 37] for terms similar to $SR_m(\boldsymbol{B}_k \times \delta\boldsymbol{u}, \boldsymbol{B}_k \times \boldsymbol{v})$ in the momentum equation. The authors derived the terms in different ways.

To demonstrate the robustness of the preconditioner in (24), in view of the definition of $\hat{\mathbb{X}}$, it suffices to solve the coupled problem: Find $\delta\boldsymbol{u} \in \boldsymbol{V}_h$ and $\delta\boldsymbol{B} \in \boldsymbol{C}_h$ such that

$$-S(\mathbf{curl}\,\delta\boldsymbol{B}, \boldsymbol{B}_k \times \boldsymbol{v}) + \mathcal{F}(\boldsymbol{u}_k; \delta\boldsymbol{u}, \boldsymbol{v}) = (\boldsymbol{f}, \boldsymbol{v}) \quad \forall\, \boldsymbol{v} \in \boldsymbol{V}_h, \tag{25a}$$

$$SR_m^{-1}(\mathbf{curl}\,\delta\boldsymbol{B}, \mathbf{curl}\,\boldsymbol{\varphi}) + \sigma(\delta\boldsymbol{B}, \boldsymbol{\varphi}) + S(\boldsymbol{B}_k \times \delta\boldsymbol{u}, \mathbf{curl}\,\boldsymbol{\varphi}) = 0 \quad \forall\, \boldsymbol{\varphi} \in \boldsymbol{C}_h, \tag{25b}$$

for given functions

$$\boldsymbol{u}_k = (y, \sin(x+z), 1)^\top, \quad \boldsymbol{B}_k = (\sin y + \cos z, 1 - \sin x, 1)^\top, \quad \boldsymbol{f} = (1, \sin x, 0)^\top.$$

In view of (24), we only concern the approximation of $\mathbb{K}\mathbb{C}_\sigma^{-1}\mathbb{J}^\top$ by the matrix form of $SR_m(\boldsymbol{B}_k \times \delta\boldsymbol{u}, \boldsymbol{B}_k \times \boldsymbol{v})$. Therefore, we can fix $R_e = \gamma = 1.0$ and consider different values of S, R_m, and σ. In the following, we test three cases of σ

$$\sigma = 1,\ 10^{-2},\ 10^{-4},$$

and three cases of physical parameters

$$S = R_m = 1,\ 10,\ 100.$$

The computational domain is the unit cube $\Omega = (0,1)^3$.

Table 1: Number of preconditioned GMRES iterations for $\sigma = 1$.

h	DOFs for $(\boldsymbol{u}_h, \boldsymbol{B}_h)$	$S = R_m = 1$	$S = R_m = 10$	$S = R_m = 100$
0.217	2.3×10^4	4	13	88
0.108	1.7×10^5	4	13	70
0.054	1.3×10^6	4	13	62
0.027	1.0×10^7	4	13	59

Table 2: Number of preconditioned GMRES iterations for $\sigma = 10^{-2}$.

h	DOFs for $(\boldsymbol{u}_h, \boldsymbol{B}_h)$	$S = R_m = 1$	$S = R_m = 10$	$S = R_m = 100$
0.217	2.3×10^4	4	13	88
0.108	1.7×10^5	4	13	69
0.054	1.3×10^6	4	13	61
0.027	1.0×10^7	4	13	58

Table 3: Number of preconditioned GMRES iterations for $\sigma = 10^{-4}$.

h	DOFs for $(\boldsymbol{u}_h, \boldsymbol{B}_h)$	$S = R_m = 1$	$S = R_m = 10$	$S = R_m = 100$
0.217	2.3×10^4	4	13	88
0.108	1.7×10^5	4	13	69
0.054	1.3×10^6	4	13	61
0.027	1.0×10^7	4	13	58

Table 4: Number of preconditioned GMRES iterations for $\sigma = 10^{-4}$ with $\mathbb{S} = \mathbb{F}$.

h	DOFs for $(\boldsymbol{u}_h, \boldsymbol{B}_h)$	$S = R_m = 1$	$S = R_m = 10$	$S = R_m = 100$
0.217	2.3×10^4	4	13	79
0.108	1.7×10^5	4	13	88
0.054	1.3×10^6	4	13	94
0.027	1.0×10^7	4	14	96

We use preconditioned GMRES method to solve (25) and the preconditioner is set by (24). This means that we need solve the residual equations at each GMRES iteration

$$\mathbb{S}\mathbf{e}_u = \mathbf{r}_u, \qquad \mathbb{C}_\sigma \mathbf{e}_B = \mathbf{r}_B - \mathbb{J}^\top \mathbf{e}_u, \tag{26}$$

where $\mathbf{r}_B, \mathbf{r}_u$ stand for the residual vectors and $\mathbf{e}_B, \mathbf{e}_u$ stand for the error vectors. The tolerance for the relative residual of the GMRES method is set by 10^{-6}. The tolerances for solving the two sub-problems in (26) are set by 10^{-3}. From Table 1–3, we find that the convergence of the preconditioned GMRES is uniform with respect to both relaxation parameter σ and mesh size h. An interesting observation is that, for large $S = R_m$, the number of GMRES iterations even decreases when $h \to 0$. In this case, the magnetic field-fluid coupling becomes strong.

Table 4 shows the number of preconditioned GMRES iterations where the approximate Schur complement $\mathbb{S}$ is replaced with $\mathbb{F}$. It amounts to devise a block Gauss-Seidel preconditioner of $\mathbb{X}$ by dropping its left lower block

$$\begin{pmatrix} \mathbb{C}_\sigma & \mathbb{J}^\top \\ -\mathbb{J} & \mathbb{F} \end{pmatrix} \approx \begin{pmatrix} \mathbb{C}_\sigma & \mathbb{J}^\top \\ 0 & \mathbb{F} \end{pmatrix}. \tag{27}$$

Comparing Table 3 with Table 4, we find that, for large $S = R_m$, the convergence of GMRES method with this preconditioner becomes slow and deteriorates when $h \to 0$. This becomes even more apparent when solving the whole MHD system (see Table 9 for the computation of a driven cavity flow).

3.4. A preconditioner for the augmented Lagrangian Navier-Stokes equations

For Picard's linearization, (24) gives an approximation of the magnetic field-fluid coupling block, while for Newton's linearization, it is not clear how to derive a similar approximation of $\mathbb{K}\mathbb{C}_\sigma^{-1}\mathbb{J}^\top$ with $\eta = 1$. Nevertheless, we adopt the approximation in (24) for both $\eta = 0$ and $\eta = 1$.

Combining (18) and (24), this yields the approximation

$$\mathbb{A}_4 \approx \begin{pmatrix} \mathbb{C}_\sigma & \mathbb{G}^\top & \mathbb{J}^\top & 0 \\ 0 & -\sigma^{-1}\mathbb{L}_r & 0 & 0 \\ 0 & 0 & \mathbb{S} & \mathbb{B}^\top \\ 0 & 0 & \mathbb{B} & 0 \end{pmatrix}. \tag{28}$$

It is left to study the preconditioner for the lower right 2×2 block of $\mathbb{A}_6$, namely,

$$\begin{pmatrix} \mathbb{S} & \mathbb{B}^\top \\ \mathbb{B} & 0 \end{pmatrix}.$$

It amounts to solve the saddle point problem: Find $(\delta\boldsymbol{u}, \delta p) \in \boldsymbol{V}_h \times Q_h$ such that

$$\mathcal{F}(\boldsymbol{u}_k; \delta\boldsymbol{u}, \boldsymbol{v}) + S R_m(\boldsymbol{B}_k \times \delta\boldsymbol{u}, \boldsymbol{B}_k \times \boldsymbol{v}) - (\delta p, \operatorname{div} \boldsymbol{v}) = R_u(\boldsymbol{v}) \qquad \forall\, \boldsymbol{v} \in \boldsymbol{V}_h, \tag{29a}$$

$$-(\operatorname{div} \delta\boldsymbol{u}, q) = R_p(q) \qquad \forall\, q \in Q_h. \tag{29b}$$

In [3, 4], Benzi et al studied the Oseen equation ($\boldsymbol{B}_k = \mathbf{0}$ and $\eta = 0$) and proposed to use the preconditioner

$$\begin{pmatrix} \mathbb{F} & \mathbb{B}^\top \\ 0 & -\left(R_e^{-1} + \gamma\right)^{-1} \mathbb{Q}_p \end{pmatrix}^{-1}, \tag{30}$$

where $\mathbb{Q}_p$ is the mass matrix on Q_h. It is proved that the above preconditioner is efficient for relatively large Reynolds number. For $\boldsymbol{u}_k = \boldsymbol{B}_k = \mathbf{0}$ and no grad-div stabilization, we refer to [25, 26] for similar arguments applied to the Stokes equations. For $\boldsymbol{u}_k = \mathbf{0}$, the pressure mass matrix is used as a sub-block in solving time-dependent MHD equations in [27]. Inspired by them, we propose to precondition

$$\begin{pmatrix} \mathbb{S} & \mathbb{B}^\top \\ \mathbb{B} & 0 \end{pmatrix} \quad \text{by the inverse of} \quad \begin{pmatrix} \mathbb{S} & \mathbb{B}^\top \\ 0 & -\left(R_e^{-1} + \gamma\right)^{-1} \mathbb{Q}_p \end{pmatrix}. \tag{31}$$

3.5. A robust preconditioner for the linearized MHD problem

Using (28) and (31), our final preconditioner for the stiffness matrix $\mathbb{A}$ is defined by

$$\mathbb{P} = \begin{pmatrix} \mathbb{C}_\sigma & 2\mathbb{G}^\top & \mathbb{J}^\top & 0 \\ 0 & -\sigma^{-1}\mathbb{L}_r & 0 & 0 \\ 0 & 0 & \mathbb{S} & \mathbb{B}^\top \\ 0 & 0 & 0 & -\left(R_e^{-1}+\gamma\right)^{-1}\mathbb{Q}_p \end{pmatrix}^{-1}. \tag{32}$$

From Section 3.3, we know that the preconditioner is insensitive to σ. Therefore, we can fix its value in the rest of the paper by

$$\sigma = S R_m^{-1}. \tag{33}$$

This yields

$$\mathbb{C}_\sigma = \mathbb{C} + S R_m^{-1}\mathbb{M}.$$

Now we are in the position to present the preconditioned GMRES algorithm for solving the linear system (12) of the MHD problem. The idea is to use an approximation of $\mathbb{P}$ to precondition $\mathbb{A}$. For convenience in notation, given a vector $\mathbf{x}$ with size of column vector of $\mathbb{A}$, we let $(\mathbf{x}_B, \mathbf{x}_r, \mathbf{x}_u, \mathbf{x}_p)$ be the vectors which consist of entries of $\mathbf{x}$ and correspond to $(\delta\boldsymbol{B}, \delta r, \delta\boldsymbol{u}, \delta p)$ respectively.

Algorithm 1 (Preconditioned GMRES Algorithm). Given the tolerances $\varepsilon \in (0,1)$ and $\varepsilon_0 \in (0,1)$, the maximal number of GMRES iterations $N > 0$, and the initial guess $\mathbf{x}^{(0)}$ for the solution of (12). Set $k = 0$ and compute the residual vector

$$\mathbf{r}^{(k)} = \mathbf{b} - \mathbb{A}\mathbf{x}^{(k)}.$$

While $\left(k < N \;\;\&\;\; \left\|\mathbf{r}^{(k)}\right\|_2 > \varepsilon \left\|\mathbf{r}^{(0)}\right\|_2\right)$ do

1. Solve $\mathbb{Q}_p\mathbf{e}_p = -\left(R_e^{-1}+\gamma\right)\mathbf{r}_p^{(k)}$ by 8 CG iterations with the diagonal preconditioning.
2. Solve $\mathbb{S}\mathbf{e}_u = \mathbf{r}_u^{(k)} - \mathbb{B}^\top\mathbf{e}_p$ by preconditioned GMRES method with tolerance ε_0. The preconditioner is one-level additive Schwarz method with overlap 2 (see [6]).
3. Solve $\mathbb{L}_r\mathbf{e}_r = -S R_m^{-1}\mathbf{r}_r^{(k)}$ by preconditioned CG method with tolerance ε_0. The preconditioner is the algebraic multigrid method (AMG) solver (see [14]).
4. Solve $(\mathbb{C}+S R_m^{-1}\mathbb{M})\mathbf{e}_B = \mathbf{r}_B^{(k)} - \mathbb{J}^\top\mathbf{e}_u - 2\mathbb{G}^\top\mathbf{e}_r$ with tolerance ε_0. For $\eta = 0$, we use preconditioned CG method with the Hiptmair-Xu preconditioner (see [16]). For $\eta = 1$, we use preconditioned GMRES method with one-level additive Schwarz preconditioner (see [6]).
5. Update the solution in the GMRES iteration to obtain $\mathbf{x}^{(k+1)}$.
6. Set $k := k+1$ and compute the residual vector $\mathbf{r}^{(k)} = \mathbf{b} - \mathbb{A}\mathbf{x}^{(k)}$.

End while.

4. Numerical experiments

In this section, we present five numerical experiments to verify the convergence rate of finite element approximation to the AL formulation of the MHD model, to demonstrate the robustness of the preconditioner, to simulate the MHD phenomena in a lid-driven cavity, and to investigate the scalability of the solver. The parallel code is developed based on the finite element package—Parallel Hierarchical Grids (PHG) [44, 45]. All computations are carried out on the LSSC-III Cluster of the State Key Laboratory of Scientific and Engineering Computing, Chinese Academy of Sciences. The cluster consists of 282 computing nodes which are Inspur NX7140N blades and each blade consists of two Intel X5550 four-core processors.

We set the tolerances by $\varepsilon = 10^{-6}$ and $\varepsilon_0 = 10^{-3}$ in Algorithm 1. Without specifications, relative tolerances are set by 10^{-5} for all nonlinear iterations. Here we use PETSc's GMRES solver and set the maximal iteration number by $N = 200$ [2].

Example 1. *This example is to verify the convergence rate of finite element solutions.* The analytic solutions are chosen as

$$\boldsymbol{u} = (\sin z, 2\cos x, 0)^\top, \quad p = \sin y + \cos 1 - 1, \quad \boldsymbol{B} = (\cos y, 0, 0)^\top, \quad r = 0.$$

The parameters are set by $R_e = S = R_m = 1$ and $\gamma = 1$.

From Table 5–6, we find that the convergence rates for $\boldsymbol{u}_h$, p_h, $\boldsymbol{B}_h$ are given by

$$\|\boldsymbol{u} - \boldsymbol{u}_h\|_{\boldsymbol{H}^1(\Omega)} \sim O(h^2), \quad \|p - p_h\|_{L^2(\Omega)} \sim O(h^2), \quad \|\boldsymbol{B} - \boldsymbol{B}_h\|_{\boldsymbol{H}(\mathbf{curl},\Omega)} \sim O(h),$$
$$\|\boldsymbol{u} - \boldsymbol{u}_h\|_{L^2(\Omega)} \sim O(h^3), \quad \|\mathrm{div}\, \boldsymbol{u}_h\|_{L^2(\Omega)} \sim O(h^2), \quad \|\boldsymbol{B} - \boldsymbol{B}_h\|_{L^2(\Omega)} \sim O(h^2).$$

Remember that we are using the second-order Lagrange finite elements for discretizing $\boldsymbol{u}$, the first-order Lagrange finite elements for discretizing p, and the first-order Nédélec edge elements in the second family for discretizing $\boldsymbol{B}$. This means that optimal convergence rates are obtained for all variables.

Table 5: Convergence rates in energy norms. (Example 1)

h	$\|\boldsymbol{u} - \boldsymbol{u}_h\|_{H^1}$	order	$\|\mathrm{div}\, \boldsymbol{u}_h\|_{L^2}$	order	$\|\boldsymbol{B} - \boldsymbol{B}_h\|_{\boldsymbol{H}(\mathbf{curl})}$	order
0.433	2.893e-03	—	4.212e-04	—	4.811e-02	—
0.217	7.071e-04	2.033	1.192e-04	1.821	2.378e-02	1.017
0.108	1.745e-04	2.019	3.158e-05	1.916	1.182e-02	1.009
0.054	4.335e-05	2.009	8.121e-06	1.959	5.893e-03	1.004

Table 6: Convergence rates in $\boldsymbol{L}^2(\Omega)$–norms. (Example 1)

h	$\|\boldsymbol{u} - \boldsymbol{u}_h\|_{L^2}$	order	$\|p - p_h\|_{L^2}$	order	$\|\boldsymbol{B} - \boldsymbol{B}_h\|_{L^2}$	order
0.433	1.161e-04	—	1.848e-03	—	3.249e-03	—
0.217	1.439e-05	3.012	3.908e-04	2.242	8.191e-04	1.987
0.108	1.792e-06	3.005	9.197e-05	2.087	2.040e-04	2.006
0.054	2.319e-07	2.950	2.214e-05	2.055	5.015e-05	2.024

Example 2 (Driven Cavity Flow). *This example is to demonstrate the optimality of the solver with respect to the mesh size by the driven cavity flow.* The righthand side is given by $\boldsymbol{f} = \boldsymbol{0}$ and the boundary conditions are given by $\boldsymbol{g} = (g_1, 0, 0)^\top$, $\boldsymbol{B}_s = (1, 0, 0)^\top$ where $g_1 = g_1(z)$ is a continuous function and satisfies

$$g_1 = 1 \quad \text{if } z = 1; \qquad g_1 = 0 \quad \text{if } 0 \le z \le 1 - h.$$

Here h is the mesh size.

We first investigate the optimality of the solver to the number of DOFs. Table 7 shows the information for the meshes which we are using. Let us consider a difficult case for which the parameters are set by

$$R_e = R_m = 100, \qquad S = 1, \qquad \gamma = 1.$$

The relative tolerance for nonlinear iterations is set by 10^{-4} and the relative tolerance for linear solvers is set by $\varepsilon = 10^{-3}$. The criteria are also used in [37]. Let N_{picard}, N_{newton} denote the number of Picard's iterations and the number of Newton's iterations respectively. Let N_{gmres} denote the average number of preconditioned GMRES iterations for solving the linearized problem (12). Table 8 shows that N_{gmres} even decreases with respect to the number of DOFs for both Picard's method and Newton's method. This demonstrate the optimality of the linear solver and the efficiency of the preconditioner. However, for the given tolerance, Picard's method does not converge within 20 steps, while Newton's method converges within 5–6 steps. This was also observed by [37, Section 5.1.2] and is mainly due to strong convection in the magnetic induction equation for large magnetic Reynolds number.

Table 7: The mesh sizes and the numbers of DOFs. (Example 2)

Mesh	h	DOFs for $(\boldsymbol{B}_h, r_h)$	DOFs for $(\boldsymbol{u}_h, p_h)$
$\mathcal{T}_1$	0.2165	13,281	15,468
$\mathcal{T}_2$	0.1083	97,985	112,724
$\mathcal{T}_3$	0.0541	752,001	859,812
$\mathcal{T}_4$	0.0271	5,890,817	6,714,692

Table 8: Number of nonlinear iterations and average number of GMRES iterations. (Example 2)

Mesh	N_{gmres} (N_{picard})	N_{gmres} (N_{newton})
$\mathcal{T}_1$	17 (> 20)	28 (5)
$\mathcal{T}_2$	11 (> 20)	22 (5)
$\mathcal{T}_3$	7 (> 20)	17 (5)
$\mathcal{T}_4$	4 (> 20)	17 (6)

Table 9: Number of nonlinear iterations and average number of GMRES iterations. (Example 2)

Mesh	N_{gmres} (N_{picard}) with **BuBv**	N_{gmres} (N_{picard}) without **BuBv**
$\mathcal{T}_1$	47 (7)	63 (8)
$\mathcal{T}_2$	39 (7)	77 (12)
$\mathcal{T}_3$	33 (7)	168 (7)
$\mathcal{T}_4$	30 (7)	117 (7)

Next we examine the effect of the magnetic field-fluid coupling term on the performance of the preconditioner. Remember from (23) that the approximate Schur complement $\mathbb{S}$ is defined by the bilinear form

$$\mathcal{F}(\boldsymbol{u}_k; \delta\boldsymbol{u}, \boldsymbol{v}) + S R_m(\boldsymbol{B}_k \times \delta\boldsymbol{u}, \boldsymbol{B}_k \times \boldsymbol{v}).$$

As mentioned in the last paragraph of Subsection 3.3, dropping the second term gives $\mathbb{S} = \mathbb{F}$. For simplicity, we only consider Picard's method and set the parameters by

$$R_e = S = 100, \qquad R_m = 1, \qquad \gamma = 1.$$

In Table 9, we show the effectiveness of the preconditioner $\mathbb{P}$ with and without the term $\mathbf{BuBv} := S R_m(\boldsymbol{B}_k \times \delta\boldsymbol{u}, \boldsymbol{B}_k \times \boldsymbol{v})$ in $\mathbb{S}$. An interesting observation is that, with **BuBv**, N_{gmres} decays when the mesh is refined successively. However, without this term, N_{gmres} increases considerably.

Figure 1 are the 2D projections of velocity streamlines on three cross-sections of Ω at $x = 0.5$, $y = 0.5$, and $z = 0.5$ respectively. Figure 2 shows two 3D streamlines of the vortex $\boldsymbol{\omega}_h = \mathbf{curl}\, \boldsymbol{u}_h$. The left figure shows the streamline generated by the line source $\{(0.5, 0.5, z) : 0 \le z \le 1\}$ along $(0, 0, 1)$. The right figure shows the streamline generated by the line source $\{(x, 0.5, 0.5) : 0 \le x \le 1\}$ along $(-1, 0, 0)$. They show clearly the vortex structure of the fluid. Figure 3 shows the contour of the pressure p_h on the three cross-sections. Since the driving plate moves on the top of the cavity and along the positive x-direction, we find from the left and middle figures that high pressure region concentrates near the edge of the cavity $\{(1, y, 1) : 0 < y < 1\}$. Finally, Figure 4 shows the distributions of $|\boldsymbol{B}_h|$ and Figure 5 shows the distributions of $|\boldsymbol{J}_h|$ on the three cross-sections respectively.

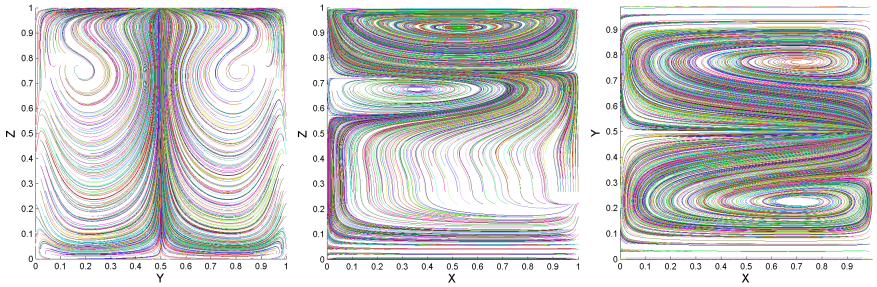

Figure 1: Streamlines of $\boldsymbol{u}_h$ at $x = 0.5$, $y = 0.5$, and $z = 0.5$ respectively (Example 2: $R_e = S = 100$, $R_m = 1$).

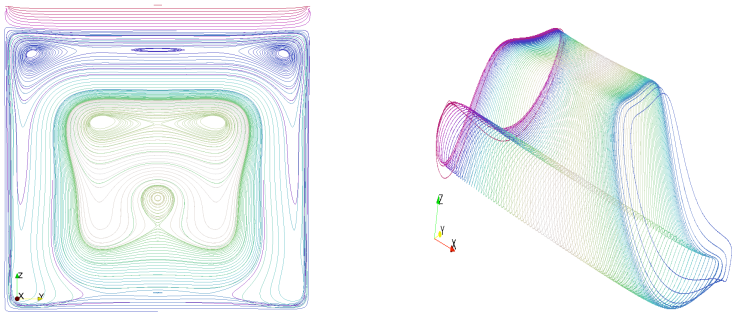

Figure 2: Two streamlines of the vortex. Left: line source along $(0, 0, 1)$. Right: line source along $(-1, 0, 0)^\top$. (Example 2)

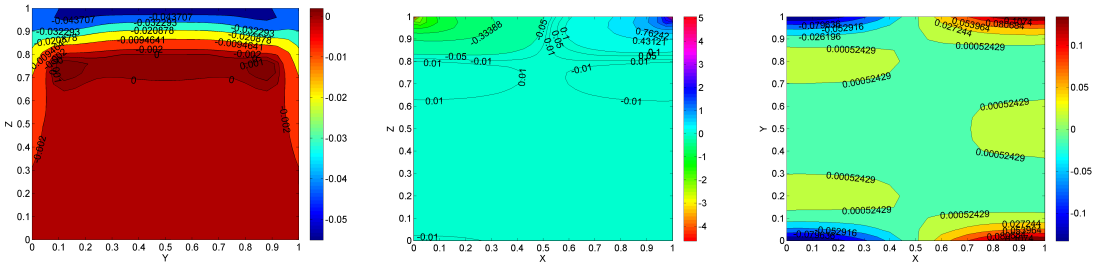

Figure 3: The contour of the pressure p_h. Left: $x = 0.5$. Middle: $y = 0.5$. Right: $z = 0.5$. (Example 2)

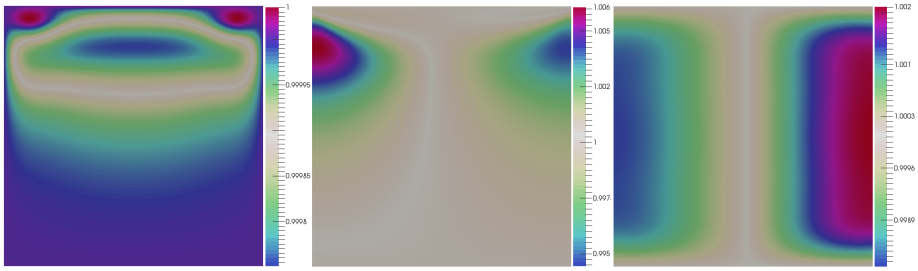

Figure 4: Distributions of $|\boldsymbol{B}_h|$ at $x = 0.5$, $y = 0.5$, and $z = 0.5$ respectively (from left to right). (Example 2)

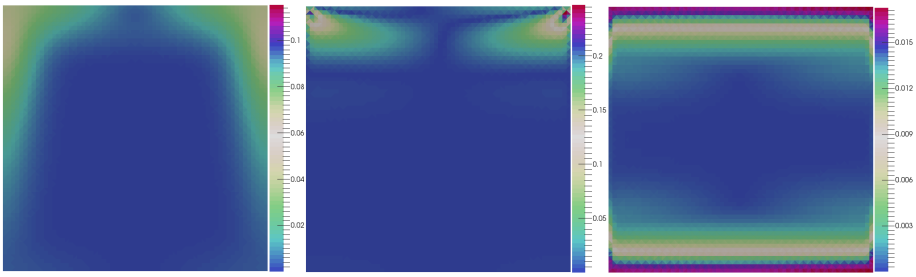

Figure 5: Distributions of $|\boldsymbol{J}_h|$ at $x = 0.5$, $y = 0.5$, and $z = 0.5$ respectively (from left to right). (Example 2)

Example 3 (Sensitivity to parameters). *This example is to examine the sensitivity of the perconditioner to physical parameters and to the grad-div stabilization parameter* γ. The setting for this example is same to that for Example 2 except that the physical parameters are different.

First we choose the computational mesh as $\mathcal{T}_3$ and set $S = \gamma = 1$. The relative tolerances are set by, as stated in the beginning of this section, 10^{-5} for nonlinear iterations and $\varepsilon = 10^{-6}$, $\varepsilon_0 = 10^{-3}$ for the linear solvers in Algorithm 1. We examine how N_{picard}, N_{newton}, and N_{gmres} vary with R_e and R_m. From Table 10, we find that the preconditioner for linear solvers is robust with respect to R_e and R_m. Moreover, Newton's method is robust for relatively large physical parameters, while Picard's method is inefficient for large magnetic Reynolds number or large Reynolds number. Particularly, for the case of $R_e = 500$, we have not found any other numerical reports on stationary driven cavity flow in the literature. Figure 6–9 show 2D streamlines of $\boldsymbol{u}_h$ on a cross-section at $y = 0.5$ for $R_e = 10$, 100, and 500 respectively. Particularly, for $R_e = 100$, Figure 7 and Figure 8 show similar vortex structures which are computed by our method and by the method in [37] respectively.

Table 10: Sensitivity to R_e and R_m. (Example 3)

	N_{gmres} (N_{picard})			N_{gmres} (N_{newton})		
R_e \ R_m	1	10	100	1	10	100
1	9 (4)	10 (12)	30 (> 20)	10 (3)	11 (4)	19 (6)
10	7 (5)	9 (13)	24 (> 20)	7 (4)	10 (4)	27 (7)
100	9 (9)	15 (11)	35 (> 20)	8 (5)	16 (5)	45 (6)
500	14 (> 20)	30 (15)	60 (> 20)	13 (7)	29 (6)	68 (6)

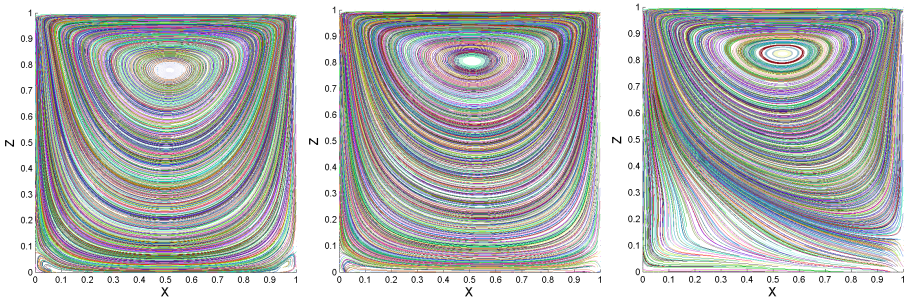

Figure 6: Streamlines of $\boldsymbol{u}_h$ at $y = 0.5$ with $R_e = 10$ and $S = 1$ (from left to right: $R_m = 1, 10, 100$). (Example 3)

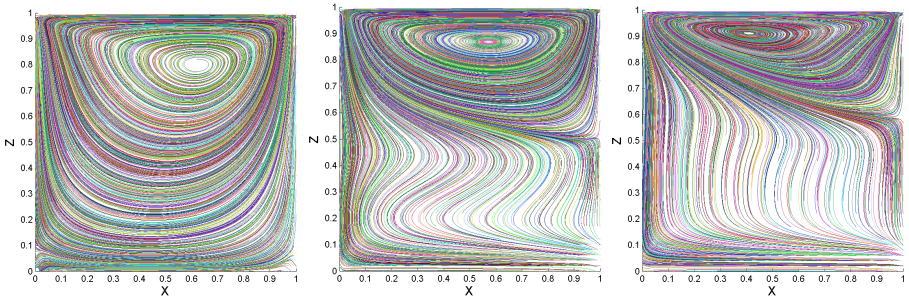

Figure 7: Streamlines of $\boldsymbol{u}_h$ at $y = 0.5$ with $R_e = 100$ and $S = 1$ (from left to right: $R_m = 1, 10, 100$). (Example 3)

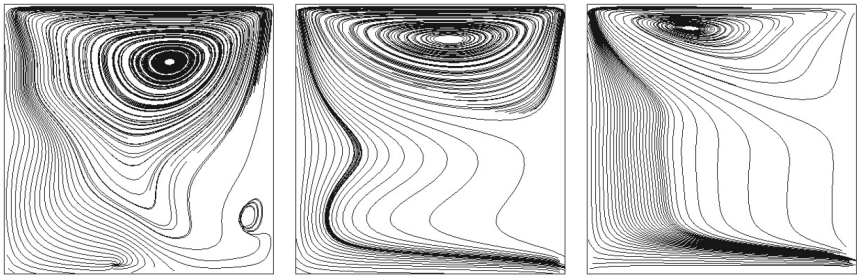

Figure 8: Streamlines of $\boldsymbol{u}_h$ in Figure 1 of [37] with $R_e = 100$ and $S = 1$ (from left to right: $R_m = 1, 10, 100$). (Example 3)

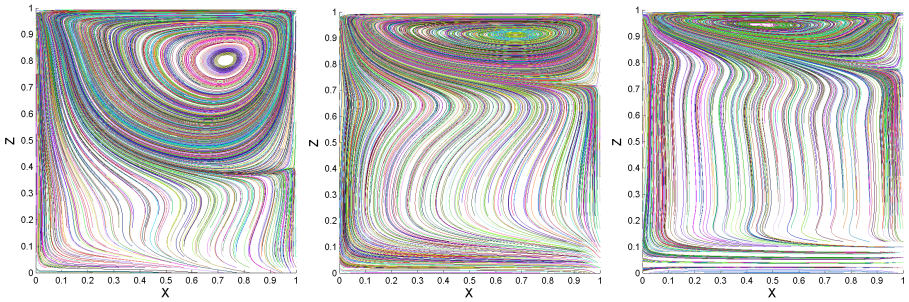

Figure 9: Streamlines of $\boldsymbol{u}_h$ at $y = 0.5$ with $R_e = 500$ and $S = 1$ (from left to right: $R_m = 1, 10, 100$). (Example 3)

Next we examine the sensitivity of the preconditioner to the grad-div stabilization parameter γ and to the mesh size. We set $R_e = 100$, $S = R_m = 10$ and investigate how the parameter γ affects the performance of solvers. Table 11 shows the number of iterations for Picard's method and Table 12 shows the number of iterations for Newton's method. We find that, at least for moderate R_m, the performances of both linear solvers and nonlinear solvers are insensitive to $\gamma = O(1)$. For $\gamma = 0$, although the number of GMRES becomes larger due to the deterioration of matrix condition, it is still optimal with respect to the number of DOFs.

Table 11: Sensitivity to γ: Picard's method. (Example 3)

Mesh	$\gamma = 0.0$	$\gamma = 0.2$	$\gamma = 0.4$	$\gamma = 0.6$	$\gamma = 1.0$	$\gamma = 1.5$
$\mathcal{T}_1$	123 (9)	58 (9)	53 (9)	51 (9)	47 (9)	45 (9)
$\mathcal{T}_2$	109 (9)	46 (10)	43 (10)	41 (10)	39 (10)	37 (10)
$\mathcal{T}_3$	95 (10)	38 (10)	35 (10)	34 (10)	32 (10)	31 (10)
$\mathcal{T}_4$	86 (10)	33 (10)	30 (10)	29 (10)	28 (10)	27 (10)

Table 12: Sensitivity to γ: Newton's method. (Example 3)

Mesh	$\gamma = 0.0$	$\gamma = 0.2$	$\gamma = 0.4$	$\gamma = 0.6$	$\gamma = 1.0$	$\gamma = 1.5$
$\mathcal{T}_1$	133 (5)	65 (4)	62 (4)	53 (5)	56 (4)	52 (4)
$\mathcal{T}_2$	119 (5)	54 (5)	50 (5)	48 (5)	43 (5)	43 (5)
$\mathcal{T}_3$	104 (5)	47 (5)	43 (5)	42 (5)	40 (5)	37 (5)
$\mathcal{T}_4$	98 (5)	42 (5)	38 (5)	37 (5)	35 (5)	33 (5)

Example 4 (Weak scalability). *This example investigates the weak scalability of the linear solver in one Picard's iteration.* The parameters are given by $R_e = S = R_m = \gamma = 1.0$.

Since one-level additive Schwarz method is unfavorable to scalability, we replace it with the Boomer-AMG preconditioner [14] in step 2 of Algorithm 1. The computations are carried out over three successively refined meshes whose sizes satisfy $h_{i+1} \approx h_i/2$, $i = 1, 2$. Table 13 shows the scalability of the linear solver for (12). It is not promising compared with the scalable preconditioners proposed Philips et al [37]. Table 14 shows the number of iterations for inner sub-solvers associated with matrices $\mathbb{Q}_p$, $\mathbb{S}$, $\mathbb{L}_r$, and $\mathbb{C}_\sigma$ respectively. We find that the deterioration of scalability is mainly due to solving the convection-diffusion problem

$$\mathbb{S}\mathbf{e}_u = \mathbf{r}_u^{(k)} - \mathbb{B}^\top \mathbf{e}_p. \tag{34}$$

With classical AMG preconditioner, the number of GMRES iterations increases considerably with the number of DOFs. Apart from the convection term in $\mathbb{S}$, the grad-div stabilization also affects the performance of classical AMG method. Two possible remedies for improving the scalability of the convection-diffusion solver could be either two-level additive Schwarz methods or modified AMG methods (cf. e.g. [3, 4]). We will work on the issue in the future.

Table 13: Scalability of the linear solver in the last Picard's interation. (Example 4)

Mesh	Total DOFs	Processors	N_{gmres}	Time (s)	Efficiency
$\mathcal{M}_1$	210709	1	11	30	—
$\mathcal{M}_2$	1611813	8	11	83	36%
$\mathcal{M}_3$	12605509	64	11	215	14%

Table 14: Average numbers of inner sub-solver iterations in the last Picard's interation. (Example 4)

Mesh	$\mathbb{Q}_p$	$\mathbb{S}$	$\mathbb{L}_r$	$\mathbb{C}_\sigma$
$\mathcal{M}_1$	8	11	4	7
$\mathcal{M}_2$	8	22	5	8
$\mathcal{M}_3$	8	45	5	9

Example 5 (Classical AMG for convection-diffusion problem). *This example is used to investiage AMG-preconditioned GMRES method for solving the convection-diffusion problem* (34). We focus on Picard's linearization and mainly concern how the two terms $(\boldsymbol{B}\times\boldsymbol{u}_h, \boldsymbol{B}\times\boldsymbol{v}_h)$ and $(\operatorname{div}\boldsymbol{u}_h, \operatorname{div}\boldsymbol{v}_h)$ affect the performance of the solver. It amounts to solving the variational problem: Find $\boldsymbol{u}_h \in \boldsymbol{V}_h$ such that

$$(\nabla\boldsymbol{u}_h, \nabla\boldsymbol{v}_h) + (\boldsymbol{w}\cdot\nabla\boldsymbol{u}_h, \boldsymbol{v}_h) + \beta(\boldsymbol{B}\times\boldsymbol{u}_h, \boldsymbol{B}\times\boldsymbol{v}_h) + \gamma(\operatorname{div}\boldsymbol{u}_h, \operatorname{div}\boldsymbol{v}_h) = (\boldsymbol{f}, \boldsymbol{v}_h) \quad \forall\, \boldsymbol{v}_h \in \boldsymbol{V}_h. \tag{35}$$

Here we set $\boldsymbol{w} = (\sin y, 1, 0)^\top, \boldsymbol{B} = (-1, 0, 0)^\top, \boldsymbol{f} = (1, \sin x, 0)^\top$.

The initial guess for the approximate solution is set by zero and the tolerance for the relative residual is set by 10^{-3}. At each GMRES iteration, we solve the residual equation by one iteration of V-cycle Boomer-AMG method [14]. Table 15 lists the numbers of GMRES iterations for different values of (β, γ). We find that, for small Reynolds number, the influence of $(\boldsymbol{B}\times\boldsymbol{u}_h, \boldsymbol{B}\times\boldsymbol{v}_h)$ on the solver is negligible. However, for relatively large Reynolds number, say $R_e = 100$ for instance, Example 2 shows that this term does improve the condition of the stiffness matrix. Moreover, from Table 15, we find that the grad-div stabilization term deteriorates the performance of the preconditioned GMRES method. We should resort to more effective AMG method for the convection-diffusion problem. This is beyond the scope of the present paper and will be our future work.

Table 15: Number of iterations for the Boomer-AMG preconditioned GMRES method. Example 5

DOFs for $\boldsymbol{u}_h$	$\beta = 1, \gamma = 1$	$\beta = 0, \gamma = 1$	$\beta = 1, \gamma = 0$	$\beta = 0, \gamma = 0$
107,811	16	15	8	8
823,875	35	35	11	11
6,440,067	112	115	21	21

5. Conclusions

In this paper, we propose a Newton-Krylov solver and a Picard-Krylov solver for finite element approximation of the grad-div stabilized formulation of 3D stationary MHD equations. An efficient block preconditioner is proposed for solving linearized discrete problems. By extensive numerical experiments, we demonstrate the robustness of the preconditioner for relatively large physical parameters and the optimality with respect to mesh sizes. The numerical experiments also show that the Newton-Krylov solver is more robust than the Picard-Krylov solver for large Reynolds number. The scalability of the monolithic solver is less competitive due to the sub-solver used for a convection-diffusion equation. Robust solvers for the convection-diffusion problem will be studied in the future and may improve the scalability.

Acknowledgement

We thank the anonymous referees very much for their valuable suggestions on the derivation of the preconditioner and on the numerical experiments.

References

[1] J.H. Adler et al, Monolithic Multigrid Methods for Two-Dimensional Resistive Magnetohydrodynamics, SIAM J. Sci. Comput., 38 (2016), B1-B24.

[2] S. Balay et al, PETSc Users Manual Revision 3.7, Mathematics and Computer Science Division, Argonne National Laboratory(ANL), 2016. http://www.mcs.anl.gov/petsc/

[3] M. Benzi and M.A. Olshanskii, An augmented Lagrangian-based approach to the Oseen problem, SIAM J. Sci. Comput., 28 (2006), 2095-2113.

[4] M. Benzi and Z. Wang, Analysis of augmented Lagrangian-based preconditioners for the steady incompressible Navier-Stokes equations, SIAM J. Sci. Comput., 33 (2011), 2761-2784.

[5] F. Brezzi and M. Fortin, Mixed and Hybrid Finite Element Methods, Springer Series in Computational Mathematics, 15, Springer, NewYork 1991.

[6] X. Cai and M. Sarkis, A restricted additive Schwarz preconditioner for general sparse linear systems, SIAM J. Sci. Comput., 21 (1999), 792–797.

[7] M.A. Case, V.J. Ervin, A. Linke, and L.G. Rebholz, A connection between Scott-Vogelius and grad-div stabilized Taylor-Hood FE approximations of the Navier-Stokes equations, SIAM J. Numer. Anal., 49 (2011), 1461-1481.

[8] P.A. Davidson, An Introduction to Magnetohydrodynamics, Cambridge University Press, Cambridge, 2001.

[9] H. Elman, V.E. Howle, J. Shadid, R. Shuttleworth, and R. Tuminaro, Block preconditioners based on approximate commutators, SIAM J. Sci. Comput., 27 (2006), 1651-1668.

[10] H. Elman, V.E. Howle, J. Shadid, D. Silvester, and R. Tuminaro, Least squares preconditioners for stabilized discretizations of the Navier-Stokes equations, SIAM J. Sci. Comput., 30 (2007), 290-311.

[11] H. Elman, D. Silvester, and A. Wathen, Finite Elements and Fast Iterative Solvers, with Applications in Incompressible Fluid Dynamics, 2nd Ed., Oxford University Press, Oxford, 2014.

[12] J. de Frutos, B. García-Archilla, V. John, and J. Novo, Grad-div stabilization for the evolutionary Oseen problem with inf-sup stable finite elements, J. Sci. Comput., 66 (2016), 991C1024.

[13] T. Heister and G. Rapin, Efficient augmented Lagrangian-type preconditioning for the Oseen problem using Grad-Div stabilization, Int. J. Numer. Meth. Fluids, 71 (2013), 118-134.

[14] V.E. Henson U.M. Yang, BoomerAMG: a parallel algebraic multigrid solver and preconditioner, Appl. Num. Math., 41 (2002), 155-177.

[15] R. Hiptmair, Finite elements in computational electromagnetism, Acta Numerica, 11 (2002), 237–339.

[16] R. Hiptmair and J. Xu, Nodal auxiliary space preconditioning in H(curl) and H(div) spaces, SIAM J. Numer. Anal., 45 (2007), 2483-2509.

[17] K. Hu and J. Xu, Structure-preserving finite element methods for stationary MHD models, arXiv:1503.06160v2.

[18] J.-F. Gerbeau, C.L. Bris, and T. Lelièvre, Mathematical methods for the Magnetohydrodynamics of Liquid Metals, Oxford University Press, Oxford, 2006.

[19] C. Greif, D. Li, D. Schötzau, and X. Wei, A mixed finite element method with exactly divergence-free velocities for incompressible magnetohydrodynamics, Comput. Methods Appl. Mech. Engrg., 199 (2010), 2840-2855.

[20] C. Greif and D. Schötzau, Preconditioners for the discretized time-harmonic Maxwell equations in mixed form, Numer. Linear Algebra Appl., 14 (2007), 281-297.

[21] M.D.Gunzburger, A.J. Meir, and J.S.Peterson, On the existence, uniqueness and finite element approximation of solutions of the equations of stationary incompressible magnetohydrodynamics, Math.Comp., 56 (1991), 523-563.

[22] D. Kay, D. Loghin, and A. Wathen, A preconditioner for the steady-state Navier-Stokes equations, SIAM J. Sci. Comput., 24 (2002), 237–256.

[23] D.A. Knoll and W.J. Rider, A multigrid preconditioned Newton-Krylov method, SIAM J. Sci. Comput., 21 (1999), 691-710.

[24] S. Lankalapalli, J.E. Flaherty, M.S. Shephard, and H. Strauss, An adaptive finite element method for magnetohydrodynamics, J. Comp. Phys., 225 (2007), 363–381.

[25] D. Loghin and A.J. Wathen, Analysis of preconditioners for saddle-point problems, SIAM J. Sci. Comput., 25 (2004), 2029-2049.

[26] K.A. Mardal and R. Winther, Preconditioning discretizations of systems of partial differential equations, Numer. Linear Algebra Appl., 18 (2011), 1–40.

[27] Y. Ma, K. Hu, X. Hu, and J.Xu, Robust preconditioners for incompressible MHD models, J. Comp. Phys., 316 (2016), 721–746.

[28] J.C. Nédélec, A new family of mixed finite elements in $\mathbb{R}^3$, Numer. Math., 50 (1986), 57-81.

[29] M.-J. Ni and J.-F. Li, A consistent and conservative scheme for incompressible MHD flows at a low magnetic Reynolds number. Part III: On a staggered mesh, J. Comp. Phys., 231 (2012), 281–298.

[30] M.-J. Ni, R. Munipalli, N.B. Morley, P. Huang, and M.A. Abdou, A current density conservative scheme for incompressible MHD flows at a low magnetic Reynolds number. Part I: On a rectangular collocated grid system, J. Comp. Phys., 227 (2007), 174–204.

[31] M.-J. Ni, R. Munipalli, P. Huang, N.B. Morley, and M.A. Abdou, A current density conservative scheme for incompressible MHD flows at a low magnetic Reynolds number. Part II: On an arbitrary collocated mesh, J. Comp. Phys., 227 (2007), 205–228.

[32] M.A. Olshanskii, An iterative solver for the Oseen problem and numerical solution of incompressible Navier-Stokes equations, Numer. Linear Algebra Appl., 6 (1999), 353–378.

[33] M.A. Olshanskii and A. Reusken, Grad-div stabilization for stokes equations, Math. Comp., 73 (2004), 1699–1718.

[34] M. Pernice and M.D. Tocci, A multigrid-preconditioned Newton-Krylov method for the incompressible Navier-Stokes equations, SIAM J. Sci. Comput., 23 (2001), 398-418.

[35] E.G. Philips, H.C. Elman, E.C. Cyr, J.N. Shadid, and R.P. Pawlowski, A block preconditioner for an exact penalty formulation for stationary MHD, SIAM J. Sci. Comput., 36 (2014), 930-951.

[36] E.G. Philips and H.C. Elman, A stochastic approach to uncertainty in the equations of MHD kinematics, J. Comput. Phys., 284 (2015), 334-350.

[37] E.G. Philips, J.N. Shadid, E.C. Cyr, H.C. Elman, and R.P. Pawlowski, Block preconditioners for stable mixed nodal and edge finite element representations of incompressible resistive MHD, SIAM J. Sci. Comput., 38 (2016), B1009-B1031.

[38] D. Schötzau, Mixed finite element methods for stationary incompressible magneto-hydrodynamics, Numer. Math., 96 (2004), 771–800.

[39] N.B. Salah, A. Soulaimani, and W.G. Habashi, A finite element method for magnetohydrodynamics, Comput. Methods Appl. Mech. Engrg., 190 (2001), 5867-5892.

[40] Syamsudhuha and D.J. Silvester, Efficient solution of the steady-state Navier-Stokes equations using a multigrid preconditioned Newton-Krylov method, Int. J. Numer. Meth. Fluids, 43 (2003), 1407-1427.

[41] G. Wittum, Multi-grid methods for Stokes and Navier-Stokes equations: (Transforming smoothers: algorithms and numerical results), Numer. Math., 54 (1989), 543-563.

[42] S. Zeng and P. Wesseling, Multigrid solution of the incompressible Navier–Stokes equations in general coordinates, SIAM J. Numer. Anal., 31 (1994), 1764–1784.

[43] S. Zeng, C. Vuik, and P. Wesseling, Numerical solution of the incompressible Navier-Stokes equations by Krylov subspace and multigrid methods, Adv. Comput. Math., 4 (1995), 27–49.

[44] L. Zhang, A parallel algorithm for adaptive local refinement of tetrahedral meshes using bisection, Numer. Math. Theor. Meth. Appl., 2 (2009), 65–89.

[45] L. Zhang, T. Cui, H. Liu, A set of symmetric quadrature rules on triangles and tetrahedra, J. Comp. Math., 27 (2009), 89–96.